Josephson current in Fe-based superconducting junctions: Theory and experiment

Josephson current in Fe-based superconducting junctions: Theory and experiment

A. V. Burmistrova
Lomonosov Moscow State University, Faculty of Physics, 1(2), Leninskie gory, GSP-1, Moscow 119991, Russian Federation;
Lomonosov Moscow State University, Skobeltsyn Institute of Nuclear Physics, 1(2), Leninskie gory, GSP-1, Moscow 119991, Russian Federation;
Moscow Institute of Physics and Technology, Dolgoprudny, Moscow 141700, Russian Federation;
and Moscow State Pedagogical University, Moscow 119992, Russian Federation

I. A. Devyatov*
Lomonosov Moscow State University, Skobeltsyn Institute of Nuclear Physics, 1(2), Leninskie gory, GSP-1, Moscow 119991, Russian Federation
and Moscow Institute of Physics and Technology, Dolgoprudny, Moscow 141700, Russian Federation

Alexander A. Golubov
Faculty of Science and Technology and MESA+ Institute of Nanotechnology, University of Twente, 7500 AE, Enschede, The Netherlands
and Moscow Institute of Physics and Technology, Dolgoprudny, Moscow 141700, Russian Federation

Keiji Yada
Department of Applied Physics, Nagoya University, Nagoya 464-8603, Japan

Yukio Tanaka
Department of Applied Physics, Nagoya University, Nagoya 464-8603, Japan
and Moscow Institute of Physics and Technology, Dolgoprudny, Moscow 141700, Russian Federation

M. Tortello and R. S. Gonnelli
Dipartimento di Scienza Applicata e Tecnologia, Politecnico di Torino, 10129, Italy

V. A. Stepanov
P. N. Lebedev Physical Institute, Russian Academy of Sciences, 119991, Moscow, Russian Federation

Xiaxin Ding and Hai-Hu Wen
Center for Superconducting Physics and Materials, National Laboratory of Solid State Microstructures and Department of Physics, Collaborative Innovation Center for Advanced Microstructures, Nanjing University, Nanjing 210093, China

L. H. Greene
Department of Physics and the Material Research Laboratory, University of Illinois at Urbana-Champaign, Urbana, Illinois 61801, USA
(Received 13 March 2015; revised manuscript received 6 May 2015; published 2 June 2015)

We present a theory of the dc Josephson effect in contacts between Fe-based and spin-singlet s-wave superconductors. The method is based on the calculation of temperature Green's function in the junction within the tight-binding model. We calculate the phase dependencies of the Josephson current for different orientations of the junction relative to the crystallographic axes of Fe-based superconductor. Further, we consider the dependence of the Josephson current on the thickness of an insulating layer and on temperature. Experimental data for $PbIn/Ba_{1-x}K_x(FeAs)_2$ point-contact Josephson junctions are consistent with theoretical predictions for $s_\pm$ symmetry of an order parameter in this material. The proposed method can be further applied to calculations of the dc Josephson current in contacts with other new unconventional multiorbital superconductors, such as Sr_2RuO_4 and the superconducting topological insulator $Cu_xBi_2Se_3$.

DOI: 10.1103/PhysRevB.91.214501 PACS number(s): 74.20.Rp, 74.70.Xa, 74.45.+c, 74.50.+r

I. INTRODUCTION

An order parameter symmetry in unconventional superconductors contains an important information about superconducting pairing mechanisms. It is well-known that the phase-sensitive tunneling experiments in junctions with unconventional superconductors provide an important information about the symmetry of the order parameter [1–4]. The theory of quasiparticle tunneling spectroscopy of a junction between a normal metal and an unconventional superconductor was developed in Refs. [5,6] and the existence of midgap Andreev bound states was predicted in Ref. [7]. The theory of a Josephson current composed of unconventional superconductor junctions was developed in Refs. [8,9]. After the discovery of high-T_C cuprates, several

*igor-devyatov@yandex.ru

new types of unconventional superconductors have been discovered. The common property of these new unconventional superconductors like Sr_2RuO_4 [10–12], Fe-based superconductors (FeBS) [13], and doped superconducting insulators $Cu_xBi_2Se_3$ [14,15] is that all of them are multiorbital materials.

All these materials have a complex single-particle excitation spectrum, and one can expect sign changing of superconducting order parameters in momentum space. The interband and intervalley scattering in these multiband unconventional superconductors significantly influences their energy spectrum. Several phenomenological theories of transport in junctions based on FeBS have been proposed in the past [16–22]. However, only recently, a microscopic theory of the quasiparticle current in a normal metal–multiband superconductor junctions was formulated [23,24], which takes into account the unusual properties of these materials. But there is still no microscopic theory to describe the Josephson current in junctions between multiband superconductors and conventional single-band spin-singlet s-wave superconductors, which goes beyond the existing phenomenological theories [18,25–27].

The aim of this paper is to propose a microscopic theory of the Josephson current in junctions based on multiband superconductors. We apply this theory to calculate the current phase relations in junctions between spin-singlet s-wave and FeBS's for different orientations. We also calculate the temperature dependencies of the critical Josephson current in these junctions. We confirm that the recently proposed phase sensitive experiment [28] is feasible to determine the symmetry of the order parameter in FeBS's. A brief account of the basic results of this paper is given in Ref. [29].

The organization of our paper is as follows. In Sec. II, we discuss the general formulation of our tight-binding approach for the calculation of the dc Josephson current in junctions with single-orbital superconductors. We demonstrate that our tight-binding approach reproduces the previous results for the Josephson effect in junctions with single-orbital superconductors. In Sec. III, we present an application of our method in the multiorbital case. We consider FeBS in the framework of the two-band model and describe the detailed procedure of the calculation of the Josephson current for in-plane and out-of-plane current directions. We consider two types of pairing symmetry in FeBS, either the $s_\pm$ or the s_{++} one. In Sec. IV, we present numerically calculated results of phase dependencies of dc Josephson current for different orientations of the junctions. We show that the c axis oriented junction can be used to distinguish between the $s_\pm$- and the s_{++}-wave types of symmetry in FeBS. We also present the temperature dependencies of the maximum Josephson current. In Sec. V, experimental data for $PbIn/Ba_{1-x}K_x(FeAs)_2$ point-contact Josephson junctions are presented that are consistent with theoretical predictions for the $s_\pm$ model. We summarize the results and formulate conclusions in Sec. VI.

II. TIGHT-BINDING MODEL FOR SINGLE-ORBITAL CASE

In this section, we formulate a Green's function approach for the calculation of dc Josephson current in single-orbital tight-binding models. First, we consider the procedure of calculation of 1D Josephson current for one-dimensional S/I/S junctions, where S is a conventional spin-singlet s-wave superconductor and I is an insulating layer. Then, we outline the same procedure for S/I/S_d junctions, where S_d is a spin-singlet single-orbital d-wave superconductor. We demonstrate that our tight-binding Green's function approach reproduces the previous results for both S/I/S and S/I/S_d Josephson current. In the end of this section, we discuss an alternative plane-wave approach for the calculation of the Josephson current.

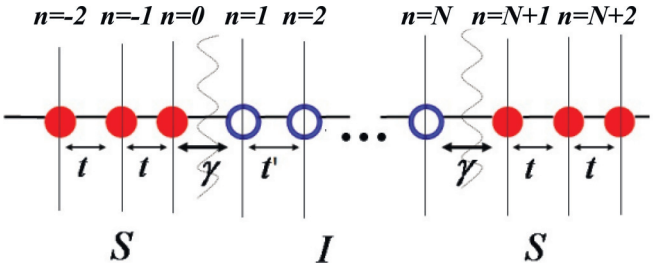

FIG. 1. (Color online) Schematic illustration of 1D model of the S/I/S Josephson junction.

A. Model of S/I/S Josephson junction

We consider the 1D tight-binding model of an S/I/S Josephson junction as depicted in Fig. 1. In the left and right parts of Fig. 1, red filled circles represent sites of s-wave superconductor S with hopping amplitude t. In the middle of Fig. 1, there are N sites of an insulator, which we represent as blue circles with hopping t' between them. At the S/I and I/S boundaries, we choose to have an equal magnitude of the hopping parameters γ in Fig. 1. We assume that the superconductors that form S/I/S Josephson junctions are the same with a common pair potential Δ_0. For simplicity, we assume that the lattice spacings a in S and I are the same and $a = 1$. To calculate the Josephson current across a S/I/S junction, we must construct a Green's function of the whole system. The simplest way to do it is to construct the Green's functions in the S,I,S regions first and then to match them at the boundaries. We define temperature Green's functions in the tight-binding model in the following form:

$$\begin{aligned} G_{n,j}(\tau_1,\tau_2) &= -\langle T_\tau c_\uparrow(n,\tau_1)c_\uparrow^+(j,\tau_2)\rangle, \\ F_{n,j}(\tau_1,\tau_2) &= \langle T_\tau c_\downarrow^+(n,\tau_1)c_\uparrow^+(j,\tau_2)\rangle, \\ \tilde{G}_{n,j}(\tau_1,\tau_2) &= -\langle T_\tau c_\downarrow^+(n,\tau_1)c_\downarrow(j,\tau_2)\rangle, \\ \tilde{F}_{n,j}(\tau_1,\tau_2) &= \langle T_\tau c_\uparrow(n,\tau_1)c_\downarrow(j,\tau_2)\rangle, \end{aligned} \tag{1}$$

with a creation (annihilation) operator $c_\sigma^+(n,\tau_i)(c_\sigma(n,\tau_i))$ of an electron with spin σ on a site n and an imaginary time ordering operator T_τ.

After the differentiation of Green's functions with respect to τ_1, one can obtain the lattice version of Gorkov's equations:

$$(i\omega-\mu)G_{n,j}^\omega - \sum_l t_{n,l}G_{l,j}^\omega + \Delta_n F_{n,j}^\omega = \delta_{n,j},$$

$$(i\omega+\mu)F_{n,j}^\omega + \sum_l t_{n,l}F_{l,j}^\omega + \Delta_n^* G_{n,j}^\omega = 0,$$

$$(i\omega-\mu)\tilde{F}^{\omega}_{n,j}-\sum_{l}t_{n,l}\tilde{F}^{\omega}_{l,j}+\Delta_n\tilde{G}^{\omega}_{n,j}=0,$$
$$(i\omega+\mu)\tilde{G}^{\omega}_{n,j}+\sum_{l}t_{n,l}\tilde{G}^{\omega}_{l,j}+\Delta^{*}_n\tilde{F}^{\omega}_{n,j}=\delta_{n,j}, \quad (2)$$

where $t_{n,l}=t$ for $l=n\pm1$, $t_{n,l}=0$ for other values of l, $\omega=\pi T(2m+1)$ is the Matsubara frequency, and T is the temperature. In the insulating region, we choose $\Delta_n=0$ in Eq. (2). One can find exact solutions of Eqs. (2) as follows:

$$\begin{pmatrix}G^{\omega,S_L}_{n,j}\\F^{\omega,S_L}_{n,j}\end{pmatrix}=a_{1j}\begin{pmatrix}\beta\\e^{i\phi}\end{pmatrix}e^{-ikn}+a_{2j}\begin{pmatrix}\beta^{-1}\\e^{i\phi}\end{pmatrix}e^{ikn} \quad (3)$$

in the left superconductor,

$$\begin{pmatrix}G^{\omega,S_R}_{n,j}\\F^{\omega,S_R}_{n,j}\end{pmatrix}=b_{1j}\begin{pmatrix}\beta\\1\end{pmatrix}e^{ikn}+b_{2j}\begin{pmatrix}1\\\beta\end{pmatrix}e^{-ikn} \quad (4)$$

in the right superconductor, and

$$\begin{aligned}\begin{pmatrix}G^{\omega,I}_{n,j}\\F^{\omega,I}_{n,j}\end{pmatrix}&=c_{1j}\begin{pmatrix}1\\0\end{pmatrix}e^{qn}+c_{2j}\begin{pmatrix}1\\0\end{pmatrix}e^{-qn}\\&+c_{3j}\begin{pmatrix}0\\1\end{pmatrix}e^{qn}+c_{4j}\begin{pmatrix}0\\1\end{pmatrix}e^{-qn}\\&-\begin{pmatrix}1\\0\end{pmatrix}\frac{e^{-q|n-j|}}{2t\sinh q}\end{aligned} \quad (5)$$

in the insulator. Here, $\beta=-i(\sqrt{\omega^2+|\Delta|^2}+\omega)/|\Delta|$, $\varphi=\varphi_R-\varphi_L$, and k (q) are the phase difference between the left and right superconductors and the momentum of a quasiparticle in the superconductor (insulator), respectively. We assumed also that in Eqs. (3)–(5) the quasiclassical approximation ($\Delta\ll\mu,t,t'$) is applied.

The unknown coefficients a_{1j}, a_{2j}, b_{1j}, b_{2j}, c_{1j}, c_{2j}, c_{3j}, and c_{4j} in Eqs. (3)–(5) can be obtained from matching the Green's functions (3)–(5) at the S/I and I/S interfaces. Boundary conditions for multiorbital metals in the tight-binding approximation have been proposed recently [23,24]. For temperature Green's functions, these boundary conditions in the quasiclassical approximation at S/I boundary have the form:

$$\begin{aligned}tG^{\omega,S_L}_{1,j}&=\gamma G^{\omega,I}_{1,j},\quad tF^{\omega,S_L}_{1,j}=\gamma F^{\omega,I}_{1,j},\\\gamma G^{\omega,S_L}_{0,j}&=t'G^{\omega,I}_{0,j},\quad \gamma F^{\omega,S_L}_{0,j}=t'F^{\omega,I}_{0,j},\end{aligned} \quad (6)$$

and the following form at I/S boundary:

$$\begin{aligned}t'G^{\omega,I}_{N+1,j}&=\gamma G^{\omega,S_R}_{N+1,j},\quad t'F^{\omega,I}_{N+1,j}=\gamma F^{\omega,S_R}_{N+1,j},\\\gamma G^{\omega,I}_{N,j}&=tG^{\omega,S_R}_{N,j},\quad \gamma F^{\omega,I}_{N,j}=tF^{\omega,S_R}_{N,j}.\end{aligned} \quad (7)$$

In the same way, one can find the other pair of Green's functions $\tilde{G}^{\omega}_{n,j}$ and $\tilde{F}^{\omega}_{n,j}$ from Eq. (2). The Josephson current across 1D S/I/S junction in the tight-binding model is given by the following expression:

$$I(\varphi)=\frac{eTt}{i\hbar}\sum_{\omega}\left(G^{\omega}_{j,j+1}-G^{\omega}_{j+1,j}+\tilde{G}^{\omega}_{j,j+1}-\tilde{G}^{\omega}_{j+1,j}\right). \quad (8)$$

Equation (8) is the generalization for the lattice model version of the Josephson current in the framework of Green's function approach.

Using Eqs. (3)–(7), it is possible to derive analytically, that previous results [30–35] for Josephson tunneling across an S/I/S constriction for equal hopping parameters in S and I with $t=t'$ are reproduced by the present tight-binding approach:

$$I(\varphi)=\frac{e\Delta_0\sigma_N\sin\varphi}{2\sqrt{1-\sigma_N\sin^2\left(\frac{\varphi}{2}\right)}}\tanh\frac{\Delta_0\sqrt{1-\sigma_N\sin^2\left(\frac{\varphi}{2}\right)}}{2T}, \quad (9)$$

where σ_N is the transparency of the S/I/S junction in the normal state. The transparency σ_N is equal to unity in the case of the direct contact ($N=0$ layers of insulator atoms) with equal hopping parameters in the bulk and at the interface, $\gamma=t$.

For the direct contact, the expression of σ_N has the following form:

$$\sigma_N=\frac{2\sigma_1^2(1-\cos 2k)}{\sigma_1^4-2\sigma_1^2\cos 2k+1}, \quad (10)$$

with $\sigma_1=t^2/\gamma^2$. In the case of $\gamma=t$ with nonzero length of an insulating region, i.e., $N\neq0$, the transparency σ_N of the S/I/S junction has the following form:

$$\sigma_N=\frac{4\sin^2k\sin^2q}{\left(\sigma_2^2+\sigma_3^2-2\sigma_2\sigma_3\cos(2qN)\right)^2}, \quad (11)$$

where $\sigma_2=1-\cos(k+q)$ and $\sigma_3=1-\cos(k+q)$.

Thus, based on our tight-binding Green's functions, Eq. (9) reproduces well-known previous results [30–35], with a generalized definition of the normal state transparency (10) and (11).

B. Model of S/I/S$_d$ Josephson junction

In this section, we extend the present tight-binding Green's functions approach to single-orbital d-wave superconductor (S_d). We consider a 2D model of an S/I/S$_d$ planar junction, where the pair potential in a d-wave superconductor has the form $\Delta=2\Delta_d(\cos k_x-\cos k_y)$ for zero misorientation angle and $\Delta=4\Delta_d\sin k_x\sin k_y$ for $\pi/4$ misorientation angle. We assume that the energy dispersion of both left and right superconductors has the form $\varepsilon_N=2t(\cos k_x+\cos k_y)+\mu_N$ and that in an insulating region $\varepsilon_I=2t(\cos k_x+\cos k_y)+\mu_I$ with $\mu_I>\mu_N$. In the actual numerical calculation, the Josepshon current is expressed by the summation of all possible values of k_y. With the increase of the thickness of the insulator N, the quasiparticles around a perpendicular injection to the insulator provide the dominant contributions to the total Josepshon current and the contribution from the large values of k_y is suppressed.

For zero misorientation angle, surface Andreev bound states are absent. For the low transparent case, the qualitative feature of the Josepshon current is similar to that of a conventional s-wave superconductor. However, for the high transparent case, the current-phase relation can deviate from the simple sinusoidal current-phase relation. Then free energy mimima can locate at $\varphi=\pm\varphi_0$, where φ_0 is neither 0 nor $\pm\pi$. The reason can be understood if we decompose the Josephson current into components with fixed k_y. For the region with small values of k_y, the obtained current phase relation is proportional to $\sin\varphi$. On the other hand, for a large magnitude

of k_y, the Josepshon current is proportional to $-\sin\varphi$. Then, after an angle averaging of k_y, the first-order term is relatively suppressed as compared to that of the second-order term proportional to $\sin 2\varphi$. Our calculations demonstrate that increasing the length of the insulating region up to $N = 3$, the current-phase relation becomes that of 0 junction. In this case, contributions to the averaged Josephson current from the regions with a large magnitude of k_y are suppressed and that from the regions with a small magnitude of k_y prevail. This feature obtained in the framework of our Green's function tight-binding approach coincides qualitatively with the previous results derived in Ref. [9] (see Fig. 2 of Ref. [9]).

Next, we study the case with a $\pi/4$ misorientation angle. It is known that the current-phase relation becomes very unusual in this case. The regions with positive and negative values of k_y give rise to different phase dependencies of the Josephson current for a fixed k_y. Positive values of k_y correspond to the 0 junction and negative ones contribute to the π junction. Then, the first-order term disappears. Then, the free-energy minima are not located at 0 or $\pm\pi$.

Our calculations demonstrate that the above feature appears even when we increase the number of insulating layers up to $N = 4$. The current-phase relation is proportional to $\sin 2\phi$ for a low transparent junction with nonzero N. These results obtained in the framework of the present lattice Green's approach coincide qualitatively with the previous results derived in Refs. [9,36] (Fig. 3 of [9]).

It is necessary to note that the same results as described above can be obtained not only in terms of Green's functions but also in terms of wave functions [37]. For this purpose, one should solve Bogoliubov-de Gennes equations and find the wave functions for an s-wave superconductor, an insulating region and a d-wave superconductor on the sites of the discrete lattice [24]. However, calculations of the total Josephson current in terms of wave functions are inconvenient for the averaging of the Josephson current over all possible values of k_y than in terms of Green's functions and lead to numerical errors. Therefore, in the following sections, we use the tight-binding Green's functions approach to obtain the averaged Josephson current in FeBS junctions.

III. MODEL FOR THE CONTACT BETWEEN S-WAVE SUPERCONDUCTOR AND A FEBS

In this section, we consider Josephson transport across S/I/S_p junctions, where S is a single-orbital s-wave superconductor, I is an insulating layer, and S_p is a FeBS. First, we consider the procedure of the calculation of the 2D Josephson current for the (100) oriented S/I/S_p junctions for zero misorientation angle. Then, we describe the same procedure for S/I/S_p junctions along c axis.

A. 2D model of the S/I/S_p Josephson junction with a (100) oriented FeBS

In Fig. 2, a two-dimensional crystallographic plane of a single-orbital s-wave superconductor S (empty circles on left side of Fig. 2), N atomic layers of an insulator (blue filled circles in the middle of Fig. 2), and a FeBS in the right part of Fig. 2 are presented. The minimal model to reproduce Fermi

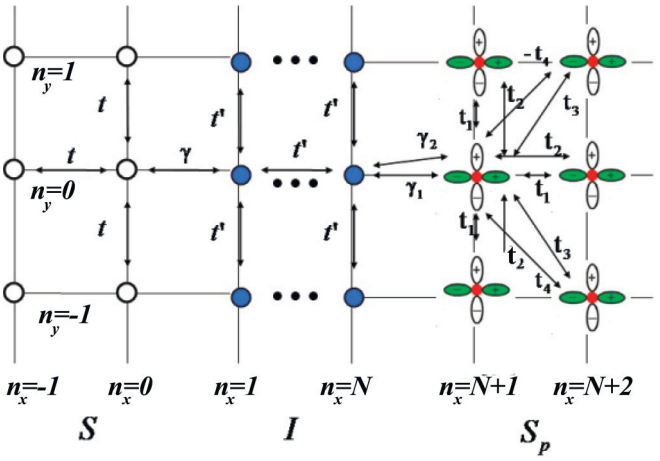

FIG. 2. (Color online) 2D tight-binding model of the (100) oriented S/I/S_p junction.

surfaces in a FeBS is a two-orbital model consists of d_{xz} and d_{yz} orbitals in iron [38]. There are four hopping parameters t_1, t_2, t_3, and t_4 in this model, as shown in Fig. 2. The Fermi surface of a FeBS in unfolded Brillouin zone is shown in Fig. 3(b).

For the pair potentials, the intraorbital $s_{\pm}$ and s_{++} models are considered [39–41]. The hopping between the sites of a single-orbital superconductor S and an insulator I is described by parameters t and t', respectively. The hopping parameter across the interface between S and I is described by γ and that between I and d_{xz} (d_{yz})-orbitals in S_p are described by γ_1 (γ_2). Due to the necessity to take into account at least two orbitals for correct description of the FeBS band structure, two hopping parameters γ_1 and γ_2 should be introduced in orbital space, which describe an interface between single-band and two-band materials (instead of a single hopping parameter γ at the interface between two single-band materials [42]). The introduction of these two parameters provides a possibility to match coherently wave functions (Green functions) at this boundary and to describe the processes of interband scaterring microscopically, as it was demonstrated in Refs. [23,24]. For simplicity, we assume that the lattice constants in S, I, and S_p are equal. To calculate the Josephson current across S/I/S_p junction, we should construct the Green's functions of the whole system (the Green's functions in S, I regions are

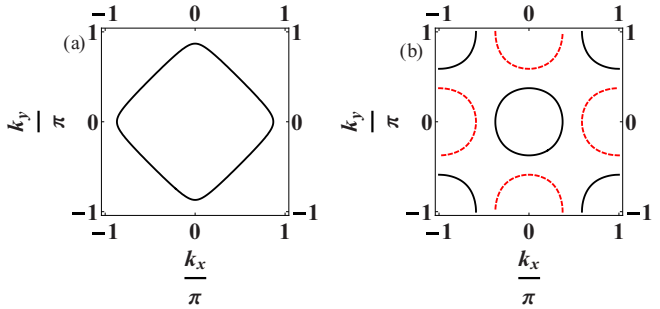

FIG. 3. (Color online) Fermi surfaces of the S/I/S_p junction with a (100) oriented FeBS. (a) Fermi surface of a single-orbital s-wave superconductor and (b) Fermi surface of a FeBS.

presented in Sec. II A [Eqs. (3) and (5)]):

$$
\begin{aligned}
G_{\{n\},\{j\}}(\tau_1,\tau_2) &= \begin{pmatrix} G^{\alpha\alpha}_{\{n\},\{j\}}(\tau_1,\tau_2) & G^{\alpha\beta}_{\{n\},\{j\}}(\tau_1,\tau_2) \\ G^{\beta\alpha}_{\{n\},\{j\}}(\tau_1,\tau_2) & G^{\beta\beta}_{\{n\},\{j\}}(\tau_1,\tau_2) \end{pmatrix} = \begin{pmatrix} -\langle T_\tau c_\uparrow(\{n\},\tau_1)c^+_\uparrow(\{j\},\tau_2)\rangle & -\langle T_\tau c_\uparrow(\{n\},\tau_1)d^+_\uparrow(\{j\},\tau_2)\rangle \\ -\langle T_\tau d_\uparrow(\{n\},\tau_1)c^+_\uparrow(\{j\},\tau_2)\rangle & -\langle T_\tau d_\uparrow(\{n\},\tau_1)d^+_\uparrow(\{j\},\tau_2)\rangle \end{pmatrix}, \\
F_{\{n\},\{j\}}(\tau_1,\tau_2) &= \begin{pmatrix} F^{\alpha\alpha}_{\{n\},\{j\}}(\tau_1,\tau_2) & F^{\alpha\beta}_{\{n\},\{j\}}(\tau_1,\tau_2) \\ F^{\beta\alpha}_{\{n\},\{j\}}(\tau_1,\tau_2) & F^{\beta\beta}_{\{n\},\{j\}}(\tau_1,\tau_2) \end{pmatrix} = \begin{pmatrix} \langle T_\tau c^+_\downarrow(\{n\},\tau_1)c^+_\uparrow(\{j\},\tau_2)\rangle & \langle T_\tau c^+_\downarrow(\{n\},\tau_1)d^+_\uparrow(\{j\},\tau_2)\rangle \\ \langle T_\tau d^+_\downarrow(\{n\},\tau_1)c^+_\uparrow(\{j\},\tau_2)\rangle & \langle T_\tau d^+_\downarrow(\{n\},\tau_1)d^+_\uparrow(\{j\},\tau_2)\rangle \end{pmatrix}, \\
\tilde{G}_{\{n\},\{j\}}(\tau_1,\tau_2) &= \begin{pmatrix} \tilde{G}^{\alpha\alpha}_{\{n\},\{j\}}(\tau_1,\tau_2) & \tilde{G}^{\alpha\beta}_{\{n\},\{j\}}(\tau_1,\tau_2) \\ \tilde{G}^{\beta\alpha}_{\{n\},\{j\}}(\tau_1,\tau_2) & \tilde{G}^{\beta\beta}_{\{n\},\{j\}}(\tau_1,\tau_2) \end{pmatrix} = \begin{pmatrix} -\langle T_\tau c^+_\downarrow(\{n\},\tau_1)c_\downarrow(\{j\},\tau_2)\rangle & -\langle T_\tau c^+_\downarrow(\{n\},\tau_1)d_\downarrow(\{j\},\tau_2)\rangle \\ -\langle T_\tau d^+_\downarrow(\{n\},\tau_1)c_\downarrow(\{j\},\tau_2)\rangle & -\langle T_\tau d^+_\downarrow(\{n\},\tau_1)d_\downarrow(\{j\},\tau_2)\rangle \end{pmatrix}, \\
\tilde{F}_{\{n\},\{j\}}(\tau_1,\tau_2) &= \begin{pmatrix} \tilde{F}^{\alpha\alpha}_{\{n\},\{j\}}(\tau_1,\tau_2) & \tilde{F}^{\alpha\beta}_{\{n\},\{j\}}(\tau_1,\tau_2) \\ \tilde{F}^{\beta\alpha}_{\{n\},\{j\}}(\tau_1,\tau_2) & \tilde{F}^{\beta\beta}_{\{n\},\{j\}}(\tau_1,\tau_2) \end{pmatrix} = \begin{pmatrix} \langle T_\tau c_\uparrow(\{n\},\tau_1)c_\downarrow(\{j\},\tau_2)\rangle & \langle T_\tau c_\uparrow(\{n\},\tau_1)d_\downarrow(\{j\},\tau_2)\rangle \\ \langle T_\tau d_\uparrow(\{n\},\tau_1)c_\downarrow(\{j\},\tau_2)\rangle & \langle T_\tau d_\uparrow(\{n\},\tau_1)d_\downarrow(\{j\},\tau_2)\rangle \end{pmatrix},
\end{aligned}
\tag{12}
$$

where $c^+_\sigma(\{n\},\tau_i)(c_\sigma(\{n\},\tau_i))$ and $d^+_\sigma(\{n\},\tau_i)(d_\sigma(\{n\},\tau_i))$ are creation (annihilation) operators for the d_{xz} and d_{yz} orbitals with spin σ at $\{n\}=(n_x,n_y)$, respectively. T_τ is the imaginary time ordering operator. Superscript $\alpha(\beta)$ corresponds to the $d_{xz}(d_{yz})$ orbital, respectively. Differentiating the Green's functions (12) with respect to τ_1, expanding them in Fourier series and using a Hamiltonian for the 2D two-orbital model of a FeBS [43], one can obtain the following Gorkov's equations:

$$
\begin{aligned}
&(i\omega-\mu)G^{\alpha\alpha,\omega}_{\{n\},\{j\}} - \sum_{\{l\}} t^{\alpha\alpha}_{\{n\},\{l\}} G^{\alpha\alpha,\omega}_{\{l\},\{j\}} - \sum_{\{l\}} t^{\alpha\beta}_{\{n\},\{l\}} G^{\alpha\beta,\omega}_{\{l\},\{j\}} + \sum_{\{l\}} \Delta_{\{n\},\{l\}} F^{\alpha\alpha,\omega}_{\{l\},\{j\}} = \delta_{\{n\},\{j\}}, \\
&(i\omega-\mu)G^{\alpha\beta,\omega}_{\{n\},\{j\}} - \sum_{\{l\}} t^{\beta\beta}_{\{n\},\{l\}} G^{\alpha\beta,\omega}_{\{l\},\{j\}} - \sum_{\{l\}} t^{\beta\alpha}_{\{n\},\{l\}} G^{\alpha\alpha,\omega}_{\{l\},\{j\}} + \sum_{\{l\}} \Delta_{\{n\},\{l\}} F^{\alpha\beta,\omega}_{\{l\},\{j\}} = 0, \\
&(i\omega+\mu)F^{\alpha\alpha,\omega}_{\{n\},\{j\}} + \sum_{\{l\}} t^{\alpha\alpha}_{\{n\},\{l\}} F^{\alpha\alpha,\omega}_{\{l\},\{j\}} + \sum_{\{l\}} t^{\alpha\beta}_{\{n\},\{l\}} F^{\alpha\beta,\omega}_{\{l\},\{j\}} + \sum_{\{l\}} \Delta^*_{\{n\},\{l\}} G^{\alpha\alpha,\omega}_{\{l\},\{j\}} = 0, \\
&(i\omega+\mu)F^{\alpha\beta,\omega}_{\{n\},\{j\}} + \sum_{\{l\}} t^{\beta\beta}_{\{n\},\{l\}} F^{\alpha\beta,\omega}_{\{l\},\{j\}} + \sum_{\{l\}} t^{\beta\alpha}_{\{n\},\{l\}} F^{\alpha\alpha,\omega}_{\{l\},\{j\}} + \sum_{\{l\}} \Delta^*_{\{n\},\{l\}} G^{\alpha\beta,\omega}_{\{l\},\{j\}} = 0, \\
&(i\omega-\mu)G^{\beta\beta,\omega}_{\{n\},\{j\}} - \sum_{\{l\}} t^{\beta\beta}_{\{n\},\{l\}} G^{\beta\beta,\omega}_{\{l\},\{j\}} - \sum_{\{l\}} t^{\beta\alpha}_{\{n\},\{l\}} G^{\beta\alpha,\omega}_{\{l\},\{j\}} + \sum_{\{l\}} \Delta_{\{n\},\{l\}} F^{\beta\beta,\omega}_{\{l\},\{j\}} = \delta_{\{n\},\{j\}}, \\
&(i\omega-\mu)G^{\beta\alpha,\omega}_{\{n\},\{j\}} - \sum_{\{l\}} t^{\alpha\alpha}_{\{n\},\{l\}} G^{\beta\alpha,\omega}_{\{l\},\{j\}} - \sum_{\{l\}} t^{\alpha\beta}_{\{n\},\{l\}} G^{\beta\beta,\omega}_{\{l\},\{j\}} + \sum_{\{l\}} \Delta_{\{n\},\{l\}} F^{\beta\alpha,\omega}_{\{l\},\{j\}} = 0, \\
&(i\omega+\mu)F^{\beta\beta,\omega}_{\{n\},\{j\}} + \sum_{\{l\}} t^{\beta\beta}_{\{n\},\{l\}} F^{\beta\beta,\omega}_{\{l\},\{j\}} + \sum_{\{l\}} t^{\beta\alpha}_{\{n\},\{l\}} F^{\beta\alpha,\omega}_{\{l\},\{j\}} + \sum_{\{l\}} \Delta^*_{\{n\},\{l\}} G^{\beta\beta,\omega}_{\{l\},\{j\}} = 0, \\
&(i\omega+\mu)F^{\beta\alpha,\omega}_{\{n\},\{j\}} + \sum_{\{l\}} t^{\alpha\alpha}_{\{n\},\{l\}} F^{\beta\alpha,\omega}_{\{l\},\{j\}} + \sum_{\{l\}} t^{\alpha\beta}_{\{n\},\{l\}} F^{\beta\beta,\omega}_{\{l\},\{j\}} + \sum_{\{l\}} \Delta^*_{\{n\},\{l\}} G^{\beta\alpha,\omega}_{\{l\},\{j\}} = 0.
\end{aligned}
\tag{13}
$$

Here, $t^{\alpha\alpha}_{\{n\},\{l\}}(t^{\beta\beta}_{\{n\},\{l\}})$ are the intraorbital hopping parameters for $d_{xz}(d_{yz})$ orbital. $t^{\alpha\beta}_{\{n\},\{l\}}(t^{\beta\alpha}_{\{n\},\{l\}})$ are the interorbital hopping parameters between the different orbitals, which have the following form:

$$
\begin{aligned}
&t^{\alpha\alpha}_{\{n_x,n_y\},\{l_x,l_y\}} = t_1 \quad \text{for} \quad l_x = n_x \pm 1, \quad l_y = n_y, \\
&t^{\alpha\alpha}_{\{n_x,n_y\},\{l_x,l_y\}} = t_2 \quad \text{for} \quad l_x = n_x, \quad l_y = n_y \pm 1, \\
&t^{\alpha\alpha}_{\{n_x,n_y\},\{l_x,l_y\}} = t_3 \quad \text{for} \quad l_x = n_x \pm 1, \quad l_y = n_y \pm 1, \\
&t^{\alpha\alpha}_{\{n_x,n_y\},\{l_x,l_y\}} = 0 \quad \text{for the other conditions on the variables} \quad l_x,n_x,l_y,n_y; \\
&t^{\beta\beta}_{\{n_x,n_y\},\{l_x,l_y\}} = t_2 \quad \text{for} \quad l_x = n_x \pm 1, \quad l_y = n_y, \\
&t^{\beta\beta}_{\{n_x,n_y\},\{l_x,l_y\}} = t_1 \quad \text{for} \quad l_x = n_x, l_y = n_y \pm 1, \\
&t^{\beta\beta}_{\{n_x,n_y\},\{l_x,l_y\}} = t_3 \quad \text{for} \quad l_x = n_x \pm 1, \quad l_y = n_y \pm 1, \\
&t^{\beta\beta}_{\{n_x,n_y\},\{l_x,l_y\}} = 0 \quad \text{for the other conditions on the variables} \quad l_x,n_x,l_y,n_y; \\
&t^{\alpha\beta}_{\{n_x,n_y\},\{l_x,l_y\}} = t^{\beta\alpha}_{\{n_x,n_y\},\{l_x,l_y\}} = t_4 \quad \text{for} \quad l_x = n_x \pm 1, \quad l_y = n_y \pm 1, \\
&t^{\alpha\beta}_{\{n_x,n_y\},\{l_x,l_y\}} = t^{\beta\alpha}_{\{n_x,n_y\},\{l_x,l_y\}} = 0 \quad \text{for the other conditions on the variables} \quad l_x,n_x,l_y,n_y.
\end{aligned}
$$

In a similar way, one can obtain the other Green's functions $\tilde{G}^{\alpha\alpha,\omega}_{\{n\},\{j\}}, \tilde{G}^{\alpha\beta,\omega}_{\{n\},\{j\}}, \tilde{G}^{\beta\alpha,\omega}_{\{n\},\{j\}}, \tilde{G}^{\beta\beta,\omega}_{\{n\},\{j\}}$ and $\tilde{F}^{\alpha\alpha,\omega}_{\{n\},\{j\}}, \tilde{F}^{\alpha\beta,\omega}_{\{n\},\{j\}}, \tilde{F}^{\beta\alpha,\omega}_{\{n\},\{j\}}$ and $\tilde{F}^{\beta\beta,\omega}_{\{n\},\{j\}}$.

Placing the source terms $\delta_{\{n\},\{j\}}$ in Eqs. (2) and (13) into the insulating region I, one can see from Eq. (13) that the four upper and four lower equations (13) coincide, with $G^{\beta\alpha,\omega}_{\{n\},\{j\}} G^{\beta\beta,\omega}_{\{n\},\{j\}}$, $F^{\beta\alpha,\omega}_{\{n\},\{j\}}$, and $F^{\beta\beta,\omega}_{\{n\},\{j\}}$ corresponding to $G^{\alpha\alpha,\omega}_{\{n\},\{j\}}$, $G^{\alpha\beta,\omega}_{\{n\},\{j\}}$, $F^{\alpha\alpha,\omega}_{\{n\},\{j\}}$, and $F^{\alpha\beta,\omega}_{\{n\},\{j\}}$, respectively. Therefore, in order to calculate the Josephson current across this S/I/S$_p$ junction, it is enough to solve only either the first four or the last four equations in (13).

Solving the first four Gorkov's equations (13), we obtain the Green's functions in the quasiclassical approximation ($\Delta_p \ll \mu, t_1, t_2, t_3, t_4$):

$$\begin{pmatrix} G^{\alpha\alpha,\omega}_{\{n\},\{j\}} \\ G^{\alpha\beta,\omega}_{\{n\},\{j\}} \\ F^{\alpha\alpha,\omega}_{\{n\},\{j\}} \\ F^{\alpha\beta,\omega}_{\{n\},\{j\}} \end{pmatrix} = a_1 \begin{pmatrix} u_0(-k_{F_1}) \\ v_0(-k_{F_1}) \\ u_0(-k_{F_1})\beta_p^{(1)}(E,\Delta(-k_{F_1},k_y)) \\ v_0(-k_{F_1})\beta_p^{(1)}(E,\Delta(-k_{F_1},k_y)) \end{pmatrix} e^{-ik_{F_1}n_x + ik_y n_y} + a_2 \begin{pmatrix} u_0(k_{F_1}) \\ v_0(k_{F_1}) \\ u_0(k_{F_1})\tilde{\beta}_p^{(1)}(E,\Delta(k_{F_1},k_y)) \\ v_0(k_{F_1})\tilde{\beta}_p^{(1)}(E,\Delta(k_{F_1},k_y)) \end{pmatrix} e^{ik_{F_1}n_x + ik_y n_y}$$
$$+ a_3 \begin{pmatrix} u_0(-k_{F_2}) \\ v_0(-k_{F_2}) \\ u_0(-k_{F_2})\beta_p^{(2)}(E,\Delta(-k_{F_2},k_y)) \\ v_0(-k_{F_2})\beta_p^{(2)}(E,\Delta(-k_{F_2},k_y)) \end{pmatrix} e^{-ik_{F_2}n_x + ik_y n_y} + a_4 \begin{pmatrix} u_0(k_{F_2}) \\ v_0(k_{F_2}) \\ u_0(k_{F_2})\tilde{\beta}_p^{(2)}(E,\Delta(k_{F_2},k_y)) \\ v_0(k_{F_2})\tilde{\beta}_p^{(2)}(E,\Delta(k_{F_2},k_y)) \end{pmatrix} e^{ik_{F_2}n_x + ik_y n_y}, \quad (14)$$

where

$$\begin{pmatrix} u_0(k_x,k_y) \\ v_0(k_x,k_y) \end{pmatrix} = \begin{pmatrix} 1 \\ -\xi_{xx}(k_{F_i})/\xi_{xy}(k_{F_i}) \end{pmatrix} \quad (15)$$

and

$$\beta_p^{1(2)} = ie^{i\varphi} \frac{|\Delta_p(-k_{F_{1(2)}},k_y)|}{\sqrt{\omega^2 + |\Delta_p(-k_{F_{1(2)}},k_y)|^2} + \omega}, \quad \tilde{\beta}_p^{1(2)} = -ie^{i\varphi} \frac{|\Delta_p(k_{F_{1(2)}},k_y)|}{\sqrt{\omega^2 + |\Delta_p(k_{F_{1(2)}},k_y)|^2} - \omega}. \quad (16)$$

Here, $\xi_{xx} = 2t_1\cos(k_x) + 2t_2\cos(k_y) + \mu$ and $\xi_{xy} = 4t_4\sin(k_x)\sin(k_y)$ are the dispersion relation of the d_{xz} orbital and hybridization terms, respectively, μ is a chemical potential, and $k_{F_{1(2)}}$ is the momentum within the first (second) band in a FeBS. In a similar way, one can obtain the expressions for the Green's functions $\tilde{G}^{\alpha\alpha,\omega}_{\{n\},\{j\}}, \tilde{G}^{\alpha\beta,\omega}_{\{n\},\{j\}}$ and $\tilde{F}^{\alpha\alpha,\omega}_{\{n\},\{j\}}, \tilde{F}^{\alpha\beta,\omega}_{\{n\},\{j\}}$.

To build the Green's function of the whole S/I/S$_p$ junction, one should match Green's functions in S, I, and S$_p$ regions [Eqs. (3), (5), and (14)] at both S/I and I/S$_p$ interfaces. The boundary conditions for the Green's functions in the tight-binding approximation can be found in a similar way as in Refs. [23,24]. Due to the translational invariance of the structure in the direction parallel to the interface, the k_y component of the momentum is conserved. Further, due to the translational invariance of the considered structure, the subscript with index (y) corresponding to the coordinate along the boundary is omitted. Thus boundary conditions at the S/I boundary have the form given in Eq. (6). At the I/S$_p$ interface, the boundary conditions have the following form [23,24]:

$$\begin{aligned} &t_1 G^{\alpha\alpha,\omega}_{N,j} + 2t_3\cos k_y G^{\alpha\alpha,\omega}_{N,j} + 2it_4\sin k_y G^{\alpha\beta,\omega}_{N,j} = \gamma_1 G^{\omega,I}_{N,j}, \quad t_1 F^{\alpha\alpha,\omega}_{N,j} + 2t_3\cos k_y F^{\alpha\alpha,\omega}_{N,j} + 2it_4\sin k_y F^{\alpha\beta,\omega}_{N,j} = \gamma_1 F^{\omega,I}_{N,j}, \\ &t_2 G^{\alpha\beta,\omega}_{N,j} + 2t_3\cos k_y G^{\alpha\beta,\omega}_{N,j} + 2it_4\sin k_y G^{\alpha\alpha,\omega}_{N,j} = \gamma_2 G^{\omega,I}_{N,j}, \quad t_2 F^{\alpha\beta,\omega}_{N,j} + 2t_3\cos k_y F^{\alpha\beta,\omega}_{N,j} + 2it_4\sin k_y F^{\alpha\alpha,\omega}_{N,j} = \gamma_2 F^{\omega,I}_{N,j}, \\ &\gamma_1 G^{\alpha\alpha,\omega}_{N+1,j} + \gamma_2 G^{\alpha\beta,\omega}_{N+1,j} = t' G^{\omega,I}_{N+1,j}, \quad \gamma_1 F^{\alpha\alpha,\omega}_{N+1,j} + \gamma_2 F^{\alpha\beta,\omega}_{N+1,j} = t' F^{\omega,I}_{N+1,j}. \end{aligned} \quad (17)$$

A general expression for the Josephson current has the form

$$I = \frac{eTt'L'}{2i\pi\hbar} \int \sum_{\omega} \left(G^I_{j,j+1} - G^I_{j+1,j} + \tilde{G}^I_{j,j+1} - \tilde{G}^I_{j+1,j}\right) dk_y, \quad (18)$$

where t' is the hopping parameter inside the insulating region (see Fig. 2) and $L' = L/a$, L is the width of the junction.

B. 3D model of the S/I/S$_p$ Josephson junction along *c*-axis of FeBS

Now we consider Josephson current across an S/I/S$_p$ junction parallel to the c axis of FeBS.

In Fig. 4, a single-orbital s-wave superconductor S/insulator (I)/FeBS(S_p) junction along the z direction is shown. For the 3D tight-binding model of FeBS, the hopping parameter t_z between the same orbitals on the nearest neighbor sites in the z direction should be taken into account in addition to the hopping parameters t_1, t_2, t_3, t_4 in the x-y plane. The existence of this hopping t_z leads to light warping of cylindrical Fermi surface sheets in the z direction. The main property of the excitation spectrum of an FeBS as a function of k_z is that for each fixed value of $k_{||} = (k_x, k_y)$ only one band crosses the Fermi level. This means that for

each value of $k_{||}$ only one of the bands contributes to the electronic transport. In Fig. 4, γ, γ_{1z}, and γ_{2z} are hopping parameters across the S/I and I/S_p interfaces, respectively.

For the calculation of the Josephson current across the S/I/S_p junction along the z axis of FeBS, one can define the temperature Green's function of FeBS in the same way as in Eq. (12). One can obtain the same set of Gorkov's equations like (13) as in the previously considered case of the Josephson transport in the x-y plane of an FeBS, but with a different definition of the hopping parameters: $t^{11}_{\{n\},\{l\}}, t^{22}_{\{n\},\{l\}}, t^{12}_{\{n\},\{j\}}, t^{21}_{\{n\},\{j\}}$:

$$
\begin{aligned}
t^{(11)}_{\{n_x,n_y,n_z\},\{l_x,l_y,\quad l_z\}} &= t_1 \quad \text{for} \quad l_x = n_x \pm 1, \quad l_y = n_y, l_z = n_z,\\
t^{(11)}_{\{n_x,n_y,n_z\},\{l_x,l_y,l_z\}} &= t_2 \quad \text{for} \quad l_x = n_x, \quad l_y = n_y \pm 1, \quad l_z = n_z,\\
t^{(11)}_{\{n_x,n_y,n_z\},\{l_x,\quad l_y,l_z\}} &= t_3 \quad \text{for} \quad l_x = n_x \pm 1, \quad l_y = n_y \pm 1, \quad l_z = n_z,\\
t^{(11)}_{\{n_x,n_y,n_z\},\{l_x,l_y,\quad l_z\}} &= t_z \quad \text{for} \quad l_x = n_x, \quad l_y = n_y, \quad l_z = n_z \pm 1,\\
t^{(11)}_{\{n_x,n_y,n_z\},\{l_x,l_y\}} &= 0 \quad \text{for the other conditions on the variables} l_x,n_x,l_y,n_y,l_z,n_z;\\
t^{(22)}_{\{n_x,n_y,n_z\},\{l_x,l_y,l_z\}} &= t_2 \quad \text{for} \quad l_x = n_x \pm 1, \quad l_y = n_y, \quad l_z = n_z,\\
t^{(22)}_{\{n_x,\quad n_y,n_z\},\{l_x,l_y,l_z\}} &= t_1 \quad \text{for} l_x = n_x, \quad l_y = n_y \pm 1, \quad l_z = n_z,\\
t^{(22)}_{\{n_x,n_y,n_z\},\{l_x,\quad l_y,l_z\}} &= t_3 \quad \text{for} \quad l_x = n_x \pm 1, \quad l_y = n_y \pm 1, \quad l_z = n_z,\\
t^{(22)}_{\{n_x,\quad n_y,n_z\},\{l_x,l_y,l_z\}} &= t_z \quad \text{for} l_x = n_x, l_y = n_y, l_z = n_z \pm 1,\\
t^{(11)}_{\{n_x,n_y,n_z\},\{l_x,l_y\}} &= 0 \quad \text{for the other conditions on the variables} \quad l_x,n_x,l_y,n_y,l_z,n_z;\\
t^{(12)}_{\{n_x,n_y,n_z\},\{l_x,l_y,l_z\}} &= t^{(21)}_{\{n_x,n_y\},\{l_x,l_y\}} = t_4 \quad \text{for} \quad l_x = n_x \pm 1, \quad l_y = n_y \pm 1, \quad l_z = n_z,\\
t^{(12)}_{\{n_x,n_y,n_z\},\{l_x,l_y,l_z\}} &= t^{(21)}_{\{n_x,n_y\},\{l_x,l_y\}} = 0 \quad \text{for the other conditions on the variables} \quad l_x,n_x,l_y,n_y,l_z,n_z.
\end{aligned}
$$

Solving Gorkov's equations for this 3D model of an FeBS, one can obtain the Green's function in the S_p region, which has the same form as Eq. (14) in the case of the 2D model of an FeBS, but with another definition of the dispersion relation of the d_{xz} orbital ξ_{xx} in Eq. (15): $\xi_{xx} = 2t_1\cos(k_x) + 2t_2\cos(k_y) + 2t_z\cos(k_z) + \mu$. As a result, one can obtain the expressions for the components of Green's functions $\tilde{G}^{\alpha\alpha,\omega}_{\{n\},\{j\}}, \tilde{G}^{\alpha\beta,\omega}_{\{n\},\{j\}}, \tilde{G}^{\beta\alpha,\omega}_{\{n\},\{j\}}, \tilde{G}^{\beta\beta,\omega}_{\{n\},\{j\}}$ and $\tilde{F}^{\alpha\alpha,\omega}_{\{n\},\{j\}}, \tilde{F}^{\alpha\beta,\omega}_{\{n\},\{j\}}, \tilde{F}^{\beta\alpha,\omega}_{\{n\},\{j\}}, \tilde{F}^{\beta\beta,\omega}_{\{n\},\{j\}}$ for the 3D model of an FeBS. The Green's functions for S and I regions can be found in a similar way as in Sec. II A.

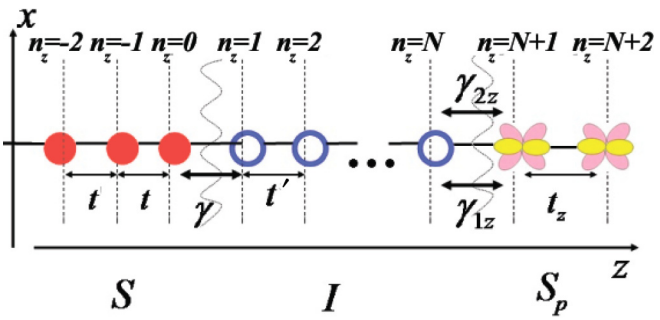

FIG. 4. (Color online) 3D tight-binding model for an S/I/S_p junction along the z axis. t', t, and t_z are hopping integrals along the z axis in S, I, and S_p, respectively. γ is the hopping integral at the S/I boundary. γ_{1z} and γ_{2z} are hopping parameters between I and S_p for xz and yz orbitals, respectively.

The boundary conditions for Green's functions in the tight-binding approximation for transport along the z axes can be found in a similar way [23,24] as in Sec. III A and they have a simpler form than in the case of transport in the x-y plane. Due to the translational invariance of the structure in the direction parallel to the interface, the $k_{||} = (k_x, k_y)$ component of the momentum is conserved. Further, due to the translational invariance of considered structure the subscripts with indices (x, y) corresponding to the coordinate of an atom in a direction parallel to the boundary is omitted. Thus the boundary conditions at the S/I boundary coincide with Eq. (6). For the I/S_p boundary we obtain the following boundary conditions in the z direction in the quasiclassical approximation $(\Delta_0, \Delta_p, \Delta'_p \ll \mu_I, \mu, \mu_N, t, t', t_1, t_2, t_3, t_4, t_z)$ [23,24]:

$$
\begin{aligned}
&t_z G^{\alpha\alpha}_{N+1,j} = \gamma_{1z} G^{I}_{N+1,j}, \quad t_z F^{\alpha\alpha}_{1,j} = \gamma_{1z} F^{I}_{N+1,j},\\
&t_z G^{\alpha\beta}_{N+1,j} = \gamma_{2z} G^{I}_{N+1,j}, \quad t_z F^{\alpha\beta}_{N+1,j} = \gamma_{2z} F^{I}_{N+1,j},\\
&\gamma_{1z} G^{\alpha\alpha}_{N,j} + \gamma_{2z} G^{\alpha\beta}_{N,j} = t G^{I}_{N,j}, \quad \gamma_{1z} F^{\alpha\alpha}_{N,j} + \gamma_{2z} F^{\alpha\beta}_{N,j} = t F^{I}_{N,j}.
\end{aligned}
\tag{19}
$$

The Josephson current across an S/I/S_p junction is described by the sum over all possible values of $k_{||}$ of Eq. (18), where k_y should be replaced by $k_{||} = (k_x, k_y)$.

IV. NUMERICAL RESULTS

In this section, we present the results of numerical calculations of the Josephson current across an S/I/S_p junction. We calculate the averaged Josephson current by summing all possible $k_{||}$ for two models of pairing symmetry in an FeBs: the

$s_{\pm}$ model with an order parameter $\Delta = 4\Delta_p \cos k_x \cos k_y$ with $\Delta_p = 0.008$ eV and the s_{++} model with an order parameter $\Delta = 2\Delta_p(\cos k_x + \cos k_y) + \Delta'_p$ with $\Delta_p = 0.001$ eV and $\Delta'_p = 0.0042$ eV. We choose $\Delta_0 = 0.002$ eV as the pair potential in S.

There is a number of factors that influence the Josephson current averaged over $k_{||}$. (1) The sensitivity of the Josephson current to the values of the hopping parameters at the I/S$_p$ interface γ_1 and γ_2. (2). The influence of the Fermi surface size of an s-wave superconductor: the Josephson current strongly depends on the values of $k_{||}$, therefore, variation of the size of the Fermi surface in S leads to changes of relative contributions to the averaged Josephson current from regions with different $k_{||}$. (3). Influence of the length of an insulating layer: increasing this length leads to the suppression of the contributions from large $k_{||}$ to the averaged Josephson current.

A. Current-phase relation in S/I/S$_p$ junctions

First, we present the results of numerical calculations of the current-phase relation (CPR) in (100) oriented S/I/S$_p$ Josephson junctions, when the charge transport occurs in the x-y planes of FeBS. We choose the normal excitation spectrum in S in the form $\varepsilon_N = 2t(\cos k_x + \cos k_y) + \mu_N$, where $t = -0.3$ and $\mu_N = 0.05$ in order to provide a large size of the Fermi surface in S. Consequently, areas with large k_y in FeBS contribute to the current (Fig. 3). We use the following values of the hopping parameters and chemical potential in FeBS: $t_1 = -0.1051$ eV, $t_2 = 0.1472$ eV, $t_3 = -0.1909$ eV, $t_4 = -0.0874$ eV, and $\mu = -0.081$ eV, according to Ref. [43], and we consider a relatively low temperature $T/T_c^s \approx 0.02$, where T_c^s is the critical temperature of the conventional s-wave superconductor. In the insulating region, we choose the normal excitation spectrum in the form of $\varepsilon_I = 2t'(\cos k_x + \cos k_y) + \mu_I$ with a hopping parameter $t' = -0.3$ eV and chemical potential $\mu_I = 1.2$ eV.

The CPR for a direct S/I/S$_p$ contact is depicted in Fig. 5, for hopping parameters across this boundary $\gamma_1 = 0.02$ and $\gamma_2 = 0.2$. Here the solid line corresponds to the total Josephson current, the dotted line corresponds to the Josephson current averaged over $k_y < \pi/2$ (over the values of k_y belonging to the hole and electron pockets of FeBS near $(k_x,k_y) = (0,0)$ and $(\pm\pi,0)$, respectively [Fig. 3(a)]), while the line with crosses

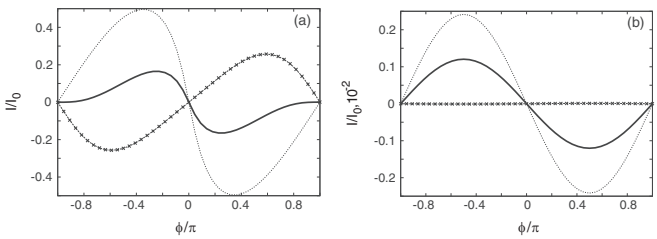

FIG. 5. The CPR for the (100) oriented S/I/S$_p$ junction for $\gamma_1 = 0.02, \gamma_2 = 0.2$, and $T/T_c^s \approx 0.02$. The solid line corresponds to the total Josephson current and the dotted line corresponds to the contribution from $|k_y| < \pi/2$. The line with crosses shows the contribution from $|k_y| > \pi/2$. $I_0 = e\Delta_0 L'/2\pi\hbar$. (a) corresponds to the direct contact and (b) corresponds to $N = 3$ atomic layers in the insulating region.

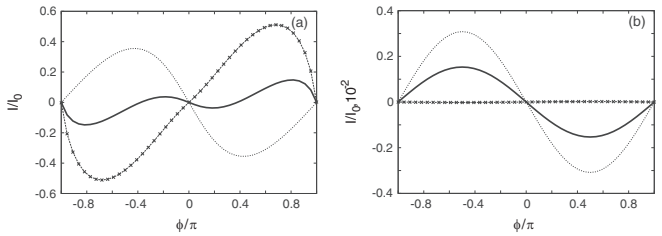

FIG. 6. The same as in Fig. 5, but $\gamma_1 = 0.02$ and $\gamma_2 = 0.3$.

corresponds to the Josephson current averaged over $k_y > \pi/2$ (the values of k_y belonging to the electron and hole pockets of a FeBS near $(k_x,k_y) = (0,\pi)$ and $(\pm\pi,\pi)$ [Fig. 3(a)]. The contributions to the Josephson current from small k_y contribute to the π coupling, while the contributions from large values of k_y to 0 contact. However, the sum of these two contributions leads to the formation of a π contact. An increase of the length of an insulating barrier up to $N = 3$ atomic layers leads to the suppression of the contributions to the averaged Josephson current from large values of k_y, therefore the contribution from small values of k_y dominates and the contact remains in the π-state for the finite length of an insulator [see Fig. 5(b)].

Figure 6(a) shows the CPR averaged over k_y for a direct S/I/S$_p$ contact for another parameter set γ_2 ($\gamma_1 = 0.02$ and $\gamma_2 = 0.3$). For these values of hopping parameters the CPR is characterized by a stable equilibrium phase $0 < \phi < \pi$, i.e., ϕ contact is realized. Increasing the length of an insulator up to $N = 3$ leads to suppression of the contributions to the averaged Josephson current from regions with large values of k_y and the π state is realized [Fig. 6(b)].

The CPR averaged over k_y for a direct S/I/S$_p$ contact is depicted in Fig. 7(a) for $\gamma_1 = 0.02$ and $\gamma_2 = 0.4$. In this case, the contribution from large k_y values to the total averaged Josephson current prevails, hence the CPR is characterized by the stable equilibrium state at phase difference $\phi = 0$ (0 contact). However, an increase of the length of an insulator up to $N = 3$ atomic layers leads to the suppression of the large k_y contributions to the averaged current and to the transition to a π state [Fig. 7(b)].

Finally, for the parameter set $\gamma_1 = 0.2$ and $\gamma_2 = 0.02$, the CPR of the direct S/I/S$_p$ contact is shown in Fig. 8(a). In this case, the opposite situation in comparison with the previous cases (Figs. 5–7) is realized, since here the contributions to the averaged current from small k_y lead to the appearance of 0 contact, while the contributions from large k_y to π contact. However, for $N = 0$, as in the case shown in Fig. 5(a), the sum of these contributions leads to the appearance of the resulting π contact, because the contribution from regions with

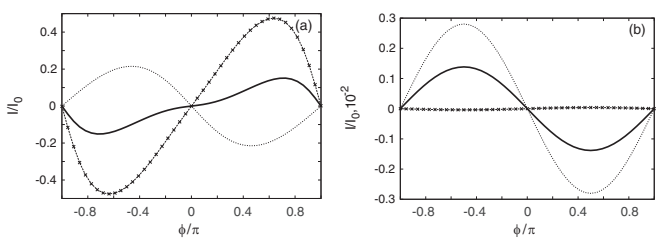

FIG. 7. The same as in Fig. 5, but $\gamma_1 = 0.02$ and $\gamma_2 = 0.4$.

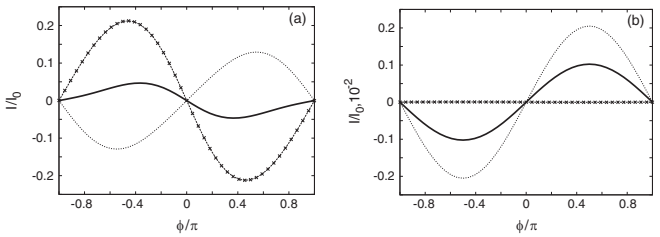

FIG. 8. The same as in Fig. 5, but $\gamma_1 = 0.2$ and $\gamma_2 = 0.02$.

large values of k_y dominates over that with small k_y. With an increase of the length of an insulator up to $N = 3$ layers, the contribution from large k_y is suppressed and the junction goes in 0 state [Fig. 8(b)].

In the case of s_{++} pairing symmetry in FeBS, the order parameter has equal signs on each Fermi surface pocket [Fig. 3(a)]. Hence, for each value of k_y and for any set of hopping amplitudes across the I/S$_p$ interface γ_1 and γ_2, we always obtain 0 contact. So, after averaging over all possible values of k_y, this S/I/S$_p$ junction has an equilibrium phase that is equal to zero. Increasing the length of an insulating layer leads to the suppression of the contributions to the averaged current from large values of k_y, but the junction still remains in 0 state.

Let us summarize the obtained results for an S/I/S$_p$ junction along (100) direction. In the case of s_{++} pairing symmetry in S_p, the junction is in 0 junction only. On the other hand, in the case of the $s_{\pm}$ symmetry, changing the interface hopping parameters, the size of the Fermi surface in the s-wave superconductor, and the insulating barrier length, we can obtain 0, π, or ϕ junctions. In the latter case, an important feature of the S/I/S$_p$ junction is the existence of a large second harmonic in CPR in a broad parameter range, as illustrated in Fig. 9. The physical origin of a large second harmonic is related to interband interference effects in the $s_{\pm}$ pairing state. These effects manifest themselves in the formation of additional current-carrying surface bound states.

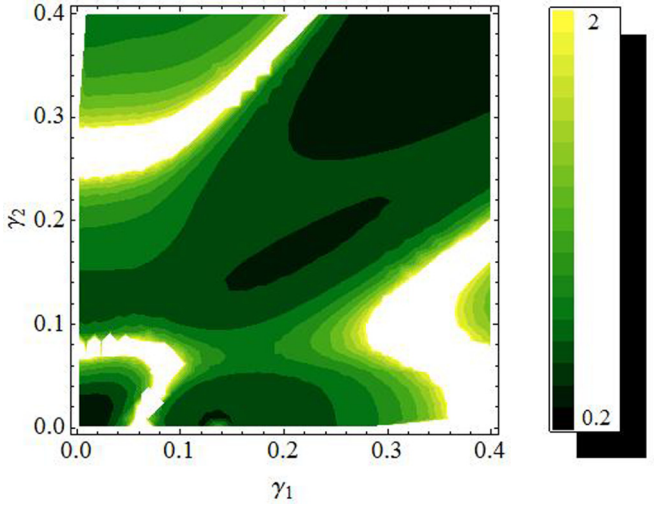

FIG. 9. (Color online) The ratio of the second and the first harmonics of the CPR for the (100) oriented S/I/S$_p$ Josephson junction for the direct contact case as a function of hopping parameters across the boundary.

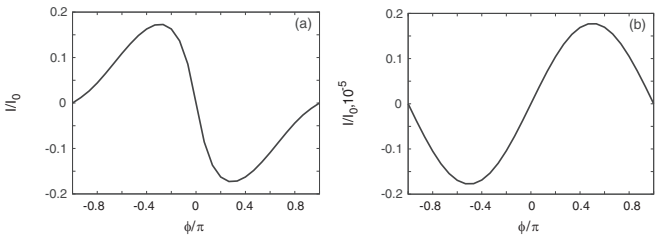

FIG. 10. The CPR of the S/I/S$_p$ Josephson junction with transport in z direction for (a) the direct contact I/S$_p$ and (b) $N = 3$ layers of an insulator atoms.

Next, we present the results of calculations of CPR in an S/I/S$_p$ junction along the z axis using the tight-binding Green's functions obtained in Sec. III B. We assume that the normal excitation spectrum in S has the form $\varepsilon_N = 2t(\cos k_x + \cos k_y + \cos k_z) + \mu_N$ with a hopping parameter $t = -0.3$ eV and a chemical potential $\mu_N = 0.6$ eV. For the chosen values of hopping parameters and chemical potential the size of the Fermi surface in S is sufficiently large and both electronic and hole pockets in FeBS contribute to the Josephson current. We choose hopping $t_z = -0.1$ eV between the same orbitals on the nearest neighbor sites of FeBS along z axis. We assume that the S/I interface is fully transparent and the I/S$_p$ interface is characterized by the following set of hopping amplitudes: $\gamma_{1z} = \gamma_{2z} = 0.17$. As in the previous case, we consider the low temperature regime: $T/T_c^s \approx 0.02$. In contrast to the case of (100) oriented S/I/S$_p$ junction, only one of the FeBS bands contributes to the Josephson current at each fixed $k_{||} = (k_x, k_y)$ for transport in the z direction.

The CPR of S/I/S$_p$ junction along the z-direction averaged over $k_{||} = (k_x, k_y)$ are plotted in Fig. 10 for the direct contact (a) and for the case of $N = 3$ insulating layers (b). In the direct contact, the main contribution to the total Josephson current stems from electronic pockets. The S/I/S$_p$ Josephson junction has a ground state at π phase difference [Fig. 10(a)]. In the presence of the insulating barrier, the main contribution to the Josephson current stems from hole pockets due to the suppression of the contributions from the regions with large $k_{||}$ to the total current. As a result, the junction has a ground state at zero phase difference [Fig. 10(b)].

Modern microfabrication techniques make it possible to create a dc SQUID loop with two different types of junctions, transparent and insulating one, attached to a c-oriented FeBS. Observation of π-phase shift in such device could provide crucial evidence for the $s_{\pm}$ symmetry in FeBS. Such experimental setup has been proposed recently in Ref. [28]. An important feature of a c-oriented S/I/S$_p$ Josephson junction is the significant suppression of the magnitude of the Josephson current in the case of a long insulating layer [Fig. 10(b)] compared to the direct contact [Fig. 10(a)]. The suppression of the Josephson current was observed in recent Josephson tunneling experiments in FeBS [44].

B. Temperature dependencies of the Josephson critical current in S/I/S$_p$ junctions

Temperature dependencies of the Josephson critical current in S/I/S$_p$ junctions were calculated in the framework of the

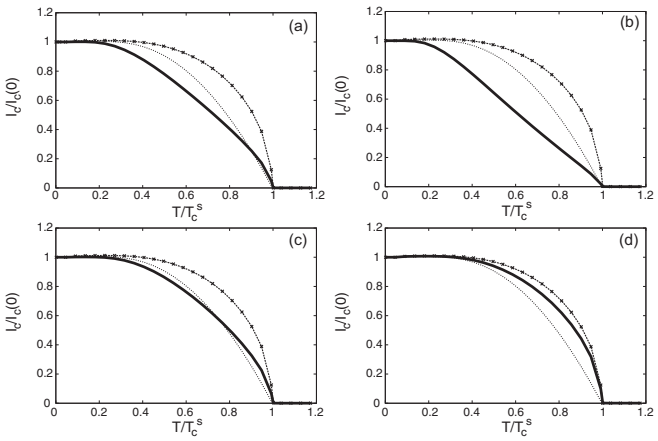

FIG. 11. The temperature dependence of the maximum Josephson current of the (100) oriented S/I/S_p junction for zero misorientation angle with respect to the interface. The solid line corresponds to the direct contact and the line with crosses corresponds to $N = 3$ insulator layers. The dashed line corresponds to the Ambegaokar-Baratoff temperature dependence of the maximum Josephson current in a conventional S/I/S junction; (a) $\gamma_1 = 0.02, \gamma_2 = 0.2$; (b) $\gamma_1 = 0.02, \gamma_2 = 0.3$; (c) $\gamma_1 = 0.02, \gamma_2 = 0.4$; and (d) $\gamma_1 = 0.2, \gamma_2 = 0.02$.

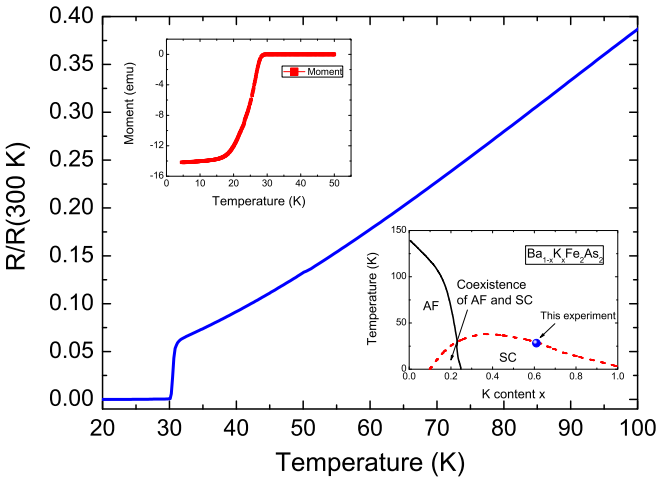

FIG. 12. (Color online) Normalized resistance $R/R(300\ \mathrm{K})$ of the $Ba_{0.4}K_{0.6}(FeAs)_2$ single crystals. (Upper inset) Zero-field cooled magnetization measurement. (Lower inset) Phase diagram of $Ba_{1-x}K_x(FeAs)_2$ [45,46]. The blue symbol represents the samples studied in this work. T_c has been determined from the magnetization curve shown in the upper inset.

developed tight-binding Green's function approach. To search for manifestations of unconventional pairing symmetry in FeBS, we considered the case of the $s_\pm$ pairing symmetry. The results are shown in Fig. 11 for the following choice of hopping parameters across the I/S_p interface: $\gamma_1 = 0.02, \gamma_2 = 0.2$ in Fig. 11(a), $\gamma_1 = 0.02, \gamma_2 = 0.3$ in Fig. 11(b), $\gamma_1 = 0.02, \gamma_2 = 0.4$ in Fig. 11(c), and $\gamma_1 = 0.2, \gamma_2 = 0.02$ in Fig. 11(d).

The solid lines in Fig. 11 correspond to the direct contact, the lines with crosses to the S/I/S_p junction with a thick insulating layer, and the dotted lines show the Ambegaokar-Baratoff [33] temperature dependence for the Josephson critical current in a standard S/I/S junction. One can see from Figs. 11(a)–11(d) that the Josephson current decreases with temperature more slowly in the case of the S/I/S_p structure with a long insulating layer compared to the S/I/S junction in the whole considered parameter range. The behavior of the critical current in S/I/S_p junctions with a direct contact depends on the choice of the hopping parameters at the I/S_p interface. The most significant difference compared to the Ambegaokar-Baratoff temperature dependence occurs in the case of $\gamma_1 = 0.02, \gamma_2 = 0.3$ [Fig. 11(b)]. This choice of hopping parameters corresponds to the realization of a nontrivial dependence of the Josephson current on the phase difference in the ground state at ϕ ($0 < \phi < \pi$) [Fig. 6(a)].

Our calculations demonstrate that the temperature dependencies of the Josephson critical current in z-axis S/I/S_p junctions, both for the direct contact and for $N = 3$ insulating layers, are quite close to each other. In both cases, $I_c(T)$ falls down with temperature more slowly than in a standard S/I/S tunnel junction.

V. EXPERIMENTAL RESULTS

The experiments were performed on $Ba_{0.4}K_{0.6}(FeAs)_2$ single crystals with $T_c \approx 30$ K. The samples were fabricated by the self-flux method. Firstly, precursor materials (BaAs, KAs, and Fe_2As) were prepared by sintering elemental mixtures at 400 °C,600 °C, and 700 °C, respectively. After a careful weighing procedure, the starting precursors with a ratio of KAs:BaAs:Fe_2As =3.6:0.4:1 were loaded into an alumina crucible and then sealed in a tantalum tube under 1 atm of argon gas. By sealing the tube in an evacuated quartz tube, the chemicals were subsequently heated up to 1050 °C and held for 5 hours. Then the furnace was cooled down to 900 °C at a rate of 3 °C/h and from 900 °C to 600 °C at 5 °C/h. Finally, the power of the furnace was shut off, and the samples were obtained by washing out the KAs flux. The EDS analysis showed that the effective composition was $Ba_{0.41}K_{0.61}Fe_{1.97}As_2$, very close to the nominal one. For this reason, we will keep referring to the samples by using the nominal content. Figure 12 shows the normalized resistance, $R/R(300\ \mathrm{K})$, from which it is possible to notice that $R(40\ \mathrm{K})/R(300\ \mathrm{K}) \approx 0.09$, in very good agreement with Ref. [45]. Moreover, since it has been shown that the $Ba_{1-x}K_x(FeAs)_2$ compounds are clean over the whole doping range [45], we can exclude any significant effect of scattering on the measured Josephson current. The lower inset of Fig. 12 reports the phase diagram for the K-doped Ba 122 materials [45,46]. The point on the diagram representative of the samples experimentally investigated in this work, shown as a blue symbol, has been obtained from the magnetization curve reported in the upper inset of Fig. 12 and matches very well with the corresponding one of the phase diagram. Finally, let us note that the samples studied here are far off the region of coexistence of antiferromagnetism and superconductivity. Hence possible effects related to such a coexistence cannot play a role.

PbIn/$Ba_{1-x}K_x(FeAs)_2$ point-contact Josephson junctions were fabricated using $Pb_{0.7}In_{0.3}$ alloy ($T_c \approx 6.5$ K, as determined by the temperature at which the Josephson current vanishes) as the counterelectrode. A sharpened tip was used for injecting the current along the c axis, while a wedgelike

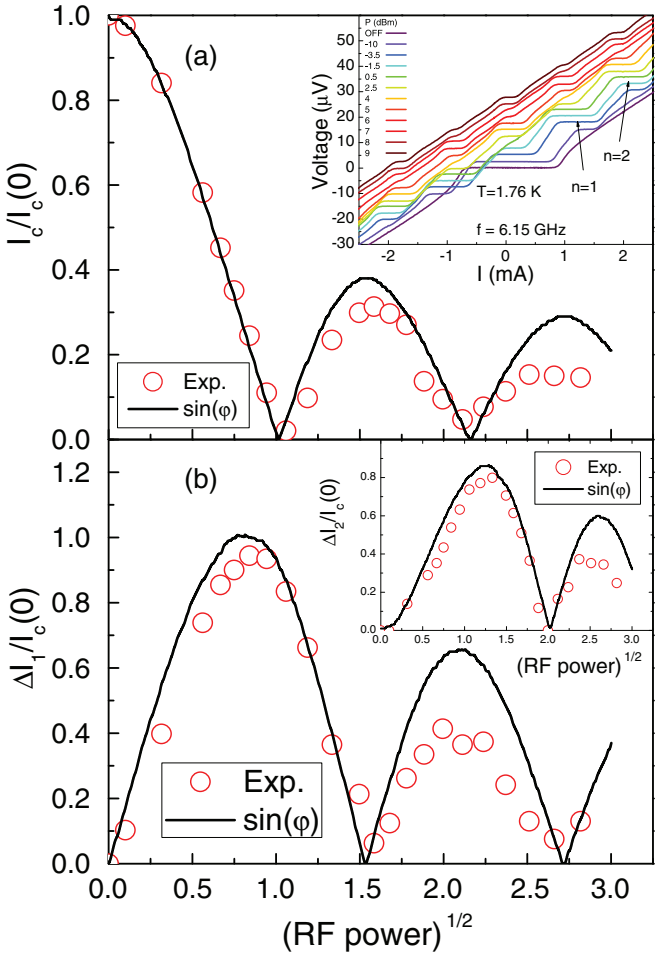

FIG. 13. (Color online) $Pb_{0.7}In_{0.3}/Ba_{0.4}K_{0.6}(FeAs)_2$ point-contact junctions with current injection along the c axis. (a) Normalized critical current as a function of the square root of the power; (inset) subset of I-V curves at $T = 1.76$ K irradiated with a 6.15-GHz rf frequency at different power levels. (b) Normalized amplitude of step 1 vs (rf power)$^{1/2}$; (inset) normalized amplitude of step 2 vs (rf power)$^{1/2}$.

one was employed for current injection along the ab plane. The contacts were formed at low temperature by means of a differential micrometer.

Reproducible, nonhysteretic RSJ-like I-V characteristics were observed at low temperature. The junctions were then irradiated with microwaves by using a monopole antenna placed at the end of a semirigid coaxial cable. The occurrence of the Josephson effect was proved by the presence of microwave-induced current steps at voltages multiple of $\hbar\omega_{\rm rf}/2e$, where $\omega_{\rm rf}$ is the microwave frequency. Subsequently, the power dependence of the current steps was investigated.

Figure 13 shows the results obtained for a c-axis junction whose I_cR_N product was about 12 μV. The inset of panel (a) reports some of the I-V curves obtained at 1.76 K and in the presence of an rf irradiation of 6.15 GHz at different power levels. It can be seen that, as expected, the amplitude of both the critical current and of the higher-order steps is modulated by changing the power. Panel (a) (symbols) shows the behavior of the critical current as a function of the square root of the power while panel (b) and the inset of panel (b) (symbols) report the amplitudes of step 1 and 2, respectively. All the steps were normalized by the low-temperature critical current.

To describe the junction under microwave irradiation, the RSJ model is extended to the nonautonomous case with an rf current-source term [47]. For the results of Fig. 13, the model has been calculated supposing $I = I_c\sin(\varphi)$ as the current-phase relation and by using the parameter $\Omega = \hbar\omega_{\rm rf}/2eI_cR_N = 1$, as imposed by the experiment. Then, since the actual microwave power coupling with the junction is unknown, a scaling parameter for the power was used to fit the data, as it is usual in these cases [48]. The lines in panel (a), (b), and the inset of panel (b) are the results of the calculations. It is worth noticing that the scaling parameter for the power is of course the same for all the current steps shown. It can be clearly seen that the agreement between the model and the experimental results is very good. This agrees also well with what is shown in Fig. 10(a), where a dominant $\sin(\varphi)$ component has been predicted for the current-phase relation along the z direction in a direct contact.

Figure 14 shows a typical result obtained for current injection along the ab plane. The inset of panel (a) reports a subset of I-V curves measured at 1.8 K and under a microwave irradiation of 3.37 GHz at different power levels. The I_cR_N product for the nonirradiated curve was approximately 15 μV. The irradiated curves show the occurrence of current-induced steps at voltages $n\hbar\omega_{\rm rf}/2e$, where n is an integer, but also at $(n/2)\hbar\omega_{\rm rf}/2e$, indicating the presence of a second-harmonic component in the current-phase relation. Also in this case the amplitude of the steps oscillates with increasing rf power.

Panel (a), (b), and the inset of panel (b) report this behavior as a function of the square root of the rf power of the amplitude of the critical current, of step 1, and of step 1/2, respectively (symbols). The data were compared to the nonautonomous case with $\Omega = 0.42$, as determined by the experiment. The equation was first solved with $I = I_c\sin(\varphi)$. The result is shown in the figure as dashed lines. This solution clearly fails in reproducing the data in amplitude but especially in following the period of the steps oscillations. Besides, the fractional steps are of course not obtained. Therefore a solution of the model with $I = I_c\sin(2\varphi)$ has been calculated as well and is shown as solid lines. In this case the fit, though not perfect, is quite close to the actual experimental behavior, especially for steps 0 and 1. Also in this case, for each expression of I, only one fitting parameter has been used for all the steps. The slight discrepancy between the model with a pure second-harmonic component and the experimental data suggests that the actual current-phase relation is not exactly $I = I_c\sin(2\varphi)$ but most probably a mixing of the first and second harmonic (see Fig. 9). The presence of a further component in the current-phase relation can be inferred, for example, by the incomplete suppression of the first minimum of the supercurrent [panel (a)] and of the first step [panel (b)] [49], as well as by the larger amplitude of the theoretical step 1/2 in the inset of panel (b). Finally, it is worth recalling that there may be, in principle, other reasons for the appearance

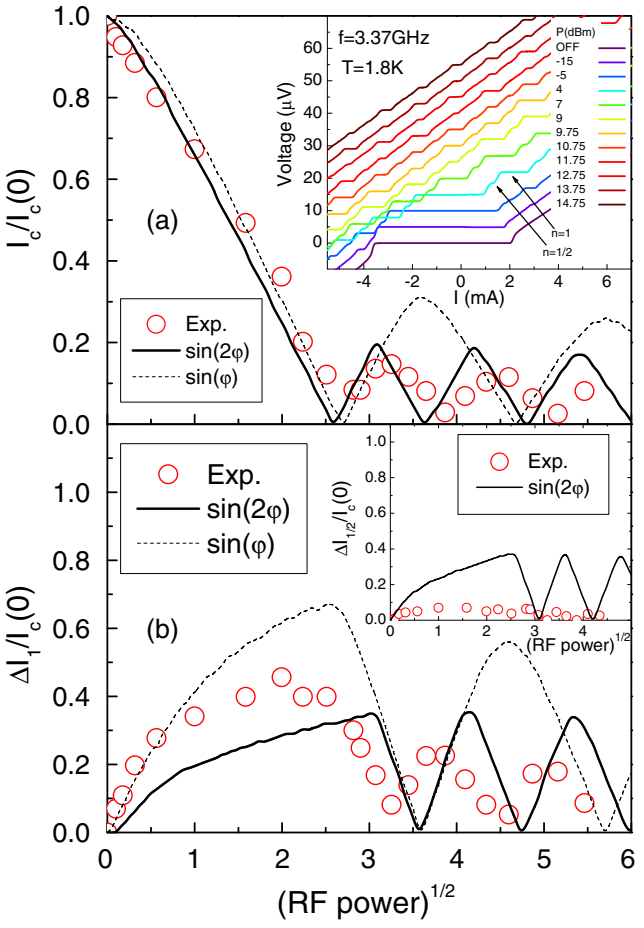

FIG. 14. (Color online) $Pb_{0.7}In_{0.3}/Ba_{0.4}K_{0.6}(FeAs)_2$ point-contact junctions with current injection along the ab plane. (a) Normalized critical current as a function of the square root of the power; (inset) subset of I-V curves at $T = 1.8$ K irradiated with a 3.37-GHz rf frequency at different power levels. (b) Normalized amplitude of step 1 vs (rf power)$^{1/2}$; (inset) normalized amplitude of step 1/2 vs (rf power)$^{1/2}$.

of subharmonic steps, but they can be excluded from playing a role here [50–52]. Possible accidental nodes in K-doped samples do not modify qualitatively the CPR of the Josephson current because, as it was demonstrated in Ref. [9], CPR is modified qualitatively only in the case of a sign-change of the order parameter. Possible nodes in K-doped samples do not imply sign-change of an order parameter.

These results indicate that a $\sin(2\varphi)$ component is highly dominant in the CPR of junctions with current injection along the ab plane. As shown in Fig. 9, this situation is predicted for a broad range of values of the hopping parameters in case of in-plane tunneling between a conventional superconductor and a multiband superconductor with an $s\pm$-wave symmetry of the order parameter. Indeed, as reported in more detail in Sec. IV, a large second-harmonic component in the CPR can occur as a consequence of interband interference effects within the $s\pm$-wave model.

Therefore these experiments appear to be in good agreement with the theoretical calculations of the Josephson current presented here in case of an $s\pm$-wave symmetry of the order parameter. However, direct measurements of the current-phase relation are desirable, in order to catch finer details of the actual current-phase relation.

VI. CONCLUSION

In this paper in the framework of a tight-binding model, we have proposed a microscopic theory describing Josephson tunneling in junctions with unusual multiband superconductors. Our theory takes into account not only the complex excitation spectrum of these superconductors, their multiband Fermi surface, interband and intervalley scattering at the boundaries, but also anisotropy and possible sign-changing of the order parameter in them. This theory has been applied to the calculation of the current-phase relation of the Josephson current and the temperature dependence of the maximum Josephson current of an FeBS/spin-singlet s-wave single-orbital superconductor junction for different orientations of the crystal axes of FeBS by changing the length of the insulating layer. We have investigated experimentally $PbIn/Ba_{1-x}K_x(FeAs)_2$ point-contact Josephson junctions and based on our theory have demonstrated that the $s_\pm$ scenario is more probable than s_{++} in $Ba_{1-x}K_x(FeAs)_2$. A largely dominant second-harmonic component in the CPR has indeed been observed in the case of current injection along the ab plane, as predicted by the theory and shown in Fig. 9. We have demonstrated theoretically that to measure the Josepshon current in the junction parallel to c axis of FeBS allows to distinguish the $s_\pm$ wave from s_{++} wave in FeBS. In the light of our theory, the recently proposed experimental setup to determine the symmetry of the order parameter in FeBS [28] has been confirmed to be plausible. It is interesting to note that our proposed theoretical scheme in the framework of a tight-binding model technique can be used for calculations of the charge transport in structures with different unconventional and complex superconductors, such as other multiband superconductors [53], superconductors on topological insulators [54–56], and superconducting topological insulators [15,57]. Also it is interesting to focus on the properties of anomalous Green's function in terms of odd-frequency pairing [58] and its relevance to topological edge states [59], since odd-frequency pairing and Majorana fermions in a multiband system are current topics of interest [54,60–63].

ACKNOWLEDGMENTS

We gratefully acknowledge T. M. Klapwijk and M. Y. Kupriyanov, D. J. Van Harlingen, and P. Seidel for valuable discussions. We thank W. K. Park, J. M. Atkinson Mora, R. W. Giannetta, and J. Ku for technical support. A.V.B. acknowledges the support by the Russian Foundation for Basic Research Project No. N14-02-31366-mol_a. A.V.B. and I.A.D. acknowledge the support by the Ministry of Education and Science of the Russian Federation Contract No. N14.B25.31.0007 and by the Russian Foundation for Basic Research Project No. N13-02-01085. A.V.B., I.A.D., and A.A.G. acknowledge the support by the Dutch FOM, by the Russian Foundation for Basic Research Project No. N15-52-50054, and by the Ministry of Education and Science of the Russian Federation Grant No. N14.587.21.0006 (RFMEFI58714X0006). V.A.S. acknowledges the Russian Academy of Sciences Division of

Physical Sciences (program 3, code 203). A.A.G. and R.S.G. acknowledge the support by the European Community through the Collaborative EU-Japan Project IRON SEA (NMP3-SL-2011–283141). M.T. acknowledges U.S.-Italy Fulbright Commission, Core Fulbright Visiting Scholar Program, during which the experimental results presented here were collected. At UIUC, the research of M.T. and L.H.G. are primarily supported by the Center for Emergent Superconductivity, Department of Energy Frontier Research Center under Grant No. DEAC0298CH1088. L.H.G. also received some support from the National Science Foundation Division of Materials Research (DMR) Award No. 12-06766.

[1] D. A. Wollman, D. J. Van Harlingen, W. C. Lee, D. M. Ginsberg, and A. J. Leggett, Phys. Rev. Lett. **71**, 2134 (1993).
[2] C. C. Tsuei, J. R. Kirtley, C. C. Chi, Lock See Yu-Jahnes, A. Gupta, T. Shaw, J. Z. Sun, and M. B. Ketchen, Phys. Rev. Lett. **73**, 593 (1994).
[3] D. J. Van Harlingen, Rev. Mod. Phys. **67**, 515 (1995).
[4] C. C. Tsuei and J. R. Kirtley, Rev. Mod. Phys. **72**, 969 (2000).
[5] Y. Tanaka and S. Kashiwaya, Phys. Rev. Lett. **74**, 3451 (1995).
[6] S. Kashiwaya and Y. Tanaka, Rep. Prog. Phys. **63**, 1641 (2000).
[7] C.-R. Hu, Phys. Rev. Lett. **72**, 1526 (1994).
[8] Y. S. Barash, H. Burkhardt, and D. Rainer, Phys. Rev. Lett. **77**, 4070 (1996).
[9] Y. Tanaka and S. Kashiwaya, Phys. Rev. B **56**, 892 (1997).
[10] Y. Maeno, H. Hashimoto, K. Yoshida, S. Nishizaki, T. Fujita, J. G. Bednorz, and F. Lichtenberg, Nature (London) **372**, 532 (1994).
[11] Z. Q. Mao, K. D. Nelson, R. Jin, Y. Liu, and Y. Maeno, Phys. Rev. Lett. **87**, 037003 (2001).
[12] S. Kashiwaya, H. Kashiwaya, H. Kambara, T. Furuta, H. Yaguchi, Y. Tanaka, and Y. Maeno, Phys. Rev. Lett. **107**, 077003 (2011).
[13] Y. Kamihara, T. Watanabe, M. Hirano, and H. Hosono, J. Am. Chem. Soc. **130**, 3296 (2008).
[14] Y. S. Hor, A. J. Williams, J. G. Checkelsky, P. Roushan, J. Seo, Q. Xu, H. W. Zandbergen, A. Yazdani, N. P. Ong, and R. J. Cava, Phys. Rev. Lett. **104**, 057001 (2010).
[15] S. Sasaki, M. Kriener, K. Segawa, K. Yada, Y. Tanaka, M. Sato, and Y. Ando, Phys. Rev. Lett. **107**, 217001 (2011).
[16] M. A. N. Araújo and P. D. Sacramento, Phys. Rev. B **79**, 174529 (2009).
[17] A. V. Burmistrova and I. A. Devyatov, JETP Lett. **95**, 239 (2012).
[18] I. B. Sperstad, J. Linder, and A. Sudbø, Phys. Rev. B **80**, 144507 (2009).
[19] A. A. Golubov, A. Brinkman, Y. Tanaka, I. I. Mazin, and O. V. Dolgov, Phys. Rev. Lett. **103**, 077003 (2009).
[20] I. A. Devyatov, M. Y. Romashka, and A. V. Burmistrova, JETP Lett. **91**, 297 (2010).
[21] A. V. Burmistrova, T. Y. Karminskaya, and I. A. Devyatov, JETP Lett. **93**, 133 (2011).
[22] A. V. Burmistrova, I. A. Devyatov, M. Y. Kupriyanov, and T. Y. Karminskaya, JETP Lett. **93**, 203 (2011).
[23] A. V. Burmistrova and I. A. Devyatov, JETP Lett. **96**, 391 (2012).
[24] A. V. Burmistrova, I. A. Devyatov, A. A. Golubov, K. Yada, and Y. Tanaka, J. Phys. Soc. Jpn **82**, 034716 (2013).
[25] E. Berg, N. H. Lindner, and T. Pereg-Barnea, Phys. Rev. Lett. **106**, 147003 (2011).
[26] W.-Q. Chen, F. Ma, Z.-Y. Lu, and F.-C. Zhang, Phys. Rev. Lett. **103**, 207001 (2009).
[27] A. E. Koshelev, Phys. Rev. B **86**, 214502 (2012).
[28] A. A. Golubov and I. I. Mazin, Appl. Phys. Lett. **102**, 032601 (2013).
[29] A. V. Burmistrova and I. A. Devyatov, Europhys. Lett. **107**, 67006 (2014).
[30] C. W. J. Beenakker and H. van Houten, Phys. Rev. Lett. **66**, 3056 (1991).
[31] I. Kulik and A. N. Omel'yanchuk, Low Temp. Phys. **3**, 459 (1977).
[32] I. Kulik and A. N. Omel'yanchuk, Low Temp. Phys. **4**, 142 (1978).
[33] V. Ambegaokar and A. Baratoff, Phys. Rev. Lett. **10**, 486 (1963).
[34] A. Furusaki and M. Tsukada, Solid State Commun. **78**, 299 (1991).
[35] P. F. Bagwell, Phys. Rev. B **46**, 12573 (1992).
[36] Y. Tanaka and S. Kashiwaya, Phys. Rev. B **53**, R11957 (1996).
[37] L.-F. Chang and P. F. Bagwell, Phys. Rev. B **49**, 15853 (1994).
[38] S. Raghu, X.-L. Qi, C.-X. Liu, D. J. Scalapino, and S.-C. Zhang, Phys. Rev. B **77**, 220503 (2008).
[39] I. I. Mazin, D. J. Singh, M. D. Johannes, and M. H. Du, Phys. Rev. Lett. **101**, 057003 (2008).
[40] K. Kuroki, S. Onari, R. Arita, H. Usui, Y. Tanaka, H. Kontani, and H. Aoki, Phys. Rev. Lett. **101**, 087004 (2008).
[41] H. Kontani and S. Onari, Phys. Rev. Lett. **104**, 157001 (2010).
[42] Q.-G. Zhu and H. Kroemer, Phys. Rev. B **27**, 3519 (1983).
[43] A. Moreo, M. Daghofer, J. A. Riera, and E. Dagotto, Phys. Rev. B **79**, 134502 (2009).
[44] P. Siedel, Superconductor Sci. Technol. **24**, 043001 (2011).
[45] Y. Liu, M. A. Tanatar, W. E. Straszheim, B. Jensen, K. W. Dennis, R. W. McCallum, V. G. Kogan, R. Prozorov, and T. A. Lograsso, Phys. Rev. B **89**, 134504 (2014).
[46] S. Avci, O. Chmaissem, D. Y. Chung, S. Rosenkranz, E. A. Goremychkin, J. P. Castellan, I. S. Todorov, J. A. Schlueter, H. Claus, A. Daoud-Aladine, D. D. Khalyavin, M. G. Kanatzidis, and R. Osborn, Phys. Rev. B **85**, 184507 (2012).
[47] A. Barone and G Paternò, *Physics and Applications of the Josephson Effect* (John Wiley and Sons, New York, 1982).
[48] H. Sellier, C. Baraduc, F. Lefloch, and R. Calemczuk, Phys. Rev. Lett. **92**, 257005 (2004).
[49] R. Kleiner, A. S. Katz, A. G. Sun, R. Summer, D. A. Gajewski, S. H. Han, S. I. Woods, E. Dantsker, B. Chen, K. Char, M. B. Maple, R. C. Dynes, and J. Clarke, Phys. Rev. Lett. **76**, 2161 (1996).
[50] E. M. Belenov, S. I. Vedeneev, G. P. Motulevich, V. A. Stepanov, and A. V. Uskov, Sov. Phys. JETP **49**, 399 (1979).
[51] P. Seidel, M. Siegel, and E. Heinz, Physica C **180**, 284 (1991).
[52] J. C. Cuevas, J. Heurich, A. Martín-Rodero, A. Levy Yeyati, and G. Schön, Phys. Rev. Lett. **88**, 157001 (2002).
[53] K. Yada, A. A. Golubov, Y. Tanaka, and S. Kashiwaya, J. Phys. Soc. Jpn. **83**, 074706 (2014).

[54] L. Fu and C. L. Kane, Phys. Rev. Lett. **100**, 096407 (2008).
[55] Y. Tanaka, T. Yokoyama, and N. Nagaosa, Phys. Rev. Lett. **103**, 107002 (2009).
[56] J. Linder, Y. Tanaka, T. Yokoyama, A. Sudbo, and N. Nagaosa, Phys. Rev. Lett. **104**, 067001 (2010).
[57] A. Yamakage, K. Yada, M. Sato, and Y. Tanaka, Phys. Rev. B **85**, 180509 (2012).
[58] Y. Tanaka and A. A. Golubov, Phys. Rev. Lett. **98**, 037003 (2007).
[59] Y. Tanaka, M. Sato, and N. Nagaosa, J. Phys. Soc. Jpn. **81**, 011013 (2012).
[60] A. M. Black-Schaffer and A. V. Balatsky, Phys. Rev. B **88**, 104514 (2013).
[61] A. M. Black-Schaffer and A. V. Balatsky, Phys. Rev. B **87**, 220506 (2013).
[62] L. Hao, P. Thalmeier, and T. K. Lee, Phys. Rev. B **84**, 235303 (2011).
[63] L. Hao, G.-L. Wang, T.-K. Lee, J. Wang, W.-F. Tsai, and Y.-H. Yang, Phys. Rev. B **89**, 214505 (2014).